J Nanostruct 9(4): 600-609, Autumn 2019

RESEARCH PAPER

Effect of Hydrothermal Reaction Temperature on the Photocatalytic Properties of $CdWO_4$-RGO Nanocomposites

*Mohammad Taghi Tourchi Moghadam[1], Mohsen Babamoradi[1], Rouhollah Azimirad[2],**

[1]*Department of Physics, Iran University of Science and Technology, Tehran, Iran*
[2]*Maleke-Ashtar University of Technology, Tehran, Iran*

ARTICLE INFO

Article History:
Received 02 May 2019
Accepted 23 June 2019
Published 01 October 2019

Keywords:
Cadmium Tungstate
Nanostructures
Photocatalyst
Reduced Graphene Oxide

ABSTRACT

Cadmium tungstate ($CdWO_4$) nanorods and $CdWO_4$-reduced graphene oxide (RGO) nanocomposites have been prepared by the hydrothermal method at 140, 160 and 180°C reaction temperatures. The synthesized samples were characterized by X-ray powder diffraction, scanning electron microscopy (SEM), Fourier transform infrared, photoluminescence spectroscopy and Raman spectroscopy. SEM image showed the pure sample consist of nanorods with 50-100 nm diameter and ~1 μm length. The images of the nanocomposite samples clearly showed existence of $CdWO_4$ nanorods and graphene sheets together. The photocatalytic activities of the as-prepared samples were investigated by degradation of methylene blue under the visible light irradiation. An enhancement in photocatalytic activity was observed with $CdWO_4$-RGO nanocomposites in compare with the pure $CdWO_4$. The effect of reaction temperature on the photocatalytic activity of the prepared nanocomposites was also investigated. The results showed that the $CdWO_4$-RGO sample which prepared at 160°C has more catalytic activity than the other samples.

How to cite this article
Tourchi Moghadam MT, Babamoradi M, Azimirad R. Effect of Hydrothermal Reaction Temperature on the Photocatalytic Properties of $CdWO_4$-RGO Nanocomposites. J Nanostruct, 2019; 9(4): 600-609. DOI: 10.22052/JNS.2019.04.001

INTRODUCTION

Extensive researches have been done on improving photocatalytic properties of materials in recent years [1-2]. Photocatalytic degradation of organic compounds can be done by some of the semiconductors in order to purify wastewater from the industries and households [3-9]. Most researches were focused on the metal oxides such as Ti, Nb, Ta, In and etc. [10-12]. It was recently reported that metal tungstates possess special physicochemical properties due to their interesting self-trapped excitations [13]. Metal tungstates were found to have a good photocatalytic properties under ultraviolet (UV) and visible light. It has been reported that $ZnWO_4$ is an efficient catalyst for dye degradation [14-15]. Therefore, significant attention has been paid to metal tungstates for their unique luminescence and structural properties [16]. One of the most practical tungstates is cadmium tungstate ($CdWO_4$). $CdWO_4$ with a monoclinic wolframite structure has high average refractive index, thermal stability, high density (7.9 gr/cm^3), low afterglow, low radiation damage and high X-ray absorption coefficient [17]. At room temperature, $CdWO_4$ with photoluminescence (PL) peak about 460 nm has been used as an X-ray scintillator [18]. The high efficiency, short decay time, high chemical stability, and high stopping power are its advantages as a scintillator material. It has also a promising application as an advanced medical X-ray detector in computerized tomography [19]. The preparation of $CdWO_4$ nanorods and nanofibers for improving the

* *Corresponding Author Email: azimirad@yahoo.com*

properties of $CdWO_4$ through hydrothermal synthesis has been reported by many groups [20-22]. Wang et al. had synthesized $CdWO_4$ nanorods by hydrothermal method. They reported a good luminescence with a PL peak at 435 nm [21]. Ye et al. have found that the $CdWO_4$ photocatalytic activities are comparable to the known $ZnWO_4$ and TiO_2 semiconductors under UV and visible light irradiation [22]. $CdWO_4$ has synthesized by various methods such as co-precipitation [23], sol–gel [24], reverse-micelle [25], solvothermal [26], solid-state metatheticreaction [27], spray pyrolysis [28], molten salt [29], and hydrothermal [20-22,30].

Hydrothermal method offers many advantages, such as mild synthesis conditions, high degree of crystallinity, high purity, and narrow particle size distribution of product. These advantages made this method as a very popular synthesis method. A lot of works have been done to enhance the photocatalytic properties of $CdWO_4$. Ye et al. reported that $CdWO_4$ doped with Eu^{+3} have better photocatalytic degradation of methyl orange (MO) than pure $CdWO_4$ [22]. Recently, Xu et al. used reduced graphene oxide (RGO) to enhance the photocatalytic properties of $CdWO_4$ [31]. They used different weight percentages of RGO and found that the $CdWO_4$-RGO with 2% RGO has the best results.

In this work, we have synthesized $CdWO_4$ with 2% RGO by hydrothermal route at different reaction temperatures as 140, 160 and 180°C. The photocatalytic activities of as-prepared samples were investigated by degradation of methylene blue (MB) under the visible light irradiation.

MATERIALS AND METHOD

The synthesis of $CdWO_4$ and $CdWO_4$-RGO have been done by hydrothermal method. For preparing $CdWO_4$, 2.198 g of $Na_2WO_4.2H_2O$ and 2.056 g of $Cd(NO_3)_2.4H_2O$ were dissolved in 30 and 20 ml of distilled water individually. Afterward, the $Na_2WO_4.2H_2O$ was added drop wise into cadmium nitrate solution. For preparing of $CdWO_4$-RGO, 0.03 ml of RGO solution (1 mg/ml) [32] added to the $CdWO_4$ solution and stringed for 20 min. Finally, suspensions were sealed into a Teflon-lined autoclave and maintained for 12 h at 180 °C for pure $CdWO_4$ and at 140, 160 and 180°C for $CdWO_4$-RGO samples named as $CdWO_4$-RGO140, $CdWO_4$-RGO160 and $CdWO_4$-RGO180, respectively. Subsequently, the autoclave was cooled to room temperature naturally. The resulting samples were washed several times with distilled water and finally with ethanol in order to remove the impurities and dried at 60°C in a vacuum oven for 24 h.

Characterizations

The crystalline structure of the prepared $CdWO_4$ and $CdWO_4$-RGO samples were analyzed by using an X-ray diffraction (XRD) (Philips-PW 1800 X-ray powder diffractometer) method with monochromatized Cu-Kα radiation (λ = 1.541874 Å) in the range of 2θ)20–40° (. The morphology of the nanostructures was depicted by a scanning electronic microscope (SEM). The SEM samples had been coated by a gold thin film using a desktop sputtering system (Nanostructured Coating Co.-Iran). Fourier transform infrared (FT-IR) spectra were recorded in the range of 400–4000 cm^{-1} using Nicolet spectrometer. Room temperature photoluminescence (PL) spectra were taken on a Perkin-Elmer LS55 equipped with a 450 W Xe lamp as an excitation source. Raman spectra were analyzed on a microscopic Raman spectrometer (SENTERRA 2009, Bruker). The concentration of MB in the irradiation process was analyzed by using a UV-visible spectrophotometer (Shimadzu, MPC-2200).

Photocatalytic measurements

In order to investigate the photocatalytic activity of the as prepared $CdWO_4$ and $CdWO_4$–RGO samples, degradation experiments of MB were performed under visible light. For this analyze, 0.01 g of samples were dispersed into a 10 mL MB solution (MB concentration: 10 mgl^{-1}) and then irradiated by visible light (400 W tungsten lamp) under continuous stirring. Before the irradiation, the suspension was maintained in the dark for 3 h to reach the complete adsorption–desorption equilibrium. All photocatalytic experiments were accomplished at the same conditions. The distance between the surface of the MB solution and the light sources were about 20 cm. The photocatalytic performance was indirectly monitored by relating the optical absorbance to the MB degradation amount using a double beam UV–visible spectrophotometer at a wavelength of 664 nm. The blank experiment without catalyst was also investigated, and its value with less than 1% degradation after 180 min illumination can be neglected.

RESULTS AND DISCUSSION

Fig. 1 shows the XRD patterns of the $CdWO_4$ and $CdWO_4$-RGO nanocomposites. All XRD peaks for the samples were indexed by monoclinic wolframite phase of $CdWO_4$ which is well consistent with the reported data (JCPDS, card No. 14-0676). The distinctive peaks for all samples centered at 2θ: 23.5, 29.1, 29.7, 30.7, 35.5 and 35.7° which are matched well with (110), (−111), (111), (020), (002), and (200) crystal planes of $CdWO_4$, respectively, which is consistent with the results of Ye et al. [33]. Lattice constants were obtained as a =5.15, b = 5.8, c = 5.13 Å and β=94.47° for all samples. The peak broadening in the XRD patterns clearly indicates that small nanocrystals are present in the samples. The results also show that the addition of RGO has no distinct effect on the crystal structure of $CdWO_4$ as reported in the Ref. [31] but XRD pattern of the pure $CdWO_4$ has sharper peaks in comparison with the $CdWO_4$-RGO nanocomposites. In order to calculate micro strains and grain size according to the Williamson-Hall equation [34], the diffraction line broadening is due to crystallite size (D) and lattice strain (ε):

$$\beta_{hkl}\cos\theta_{hkl} = \frac{k\lambda}{D} + 4\varepsilon\sin\theta_{hkl} \quad (1)$$

where λ is the X-ray wavelength (1.54 Å), k is the Scherrer constant (0.9), and ϑ is the Bragg angle. The Williamson-Hall plot is presented for $CdWO_4$-RGO140 in Fig. 2. The slope of the

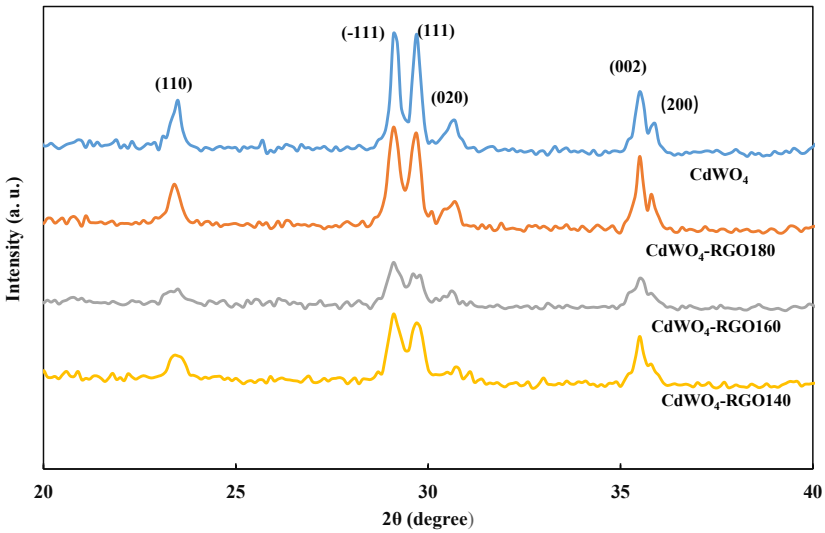

Fig. 1. XRD patterns of the pure $CdWO_4$ and $CdWO_4$-RGO140, 160 and 180 samples.

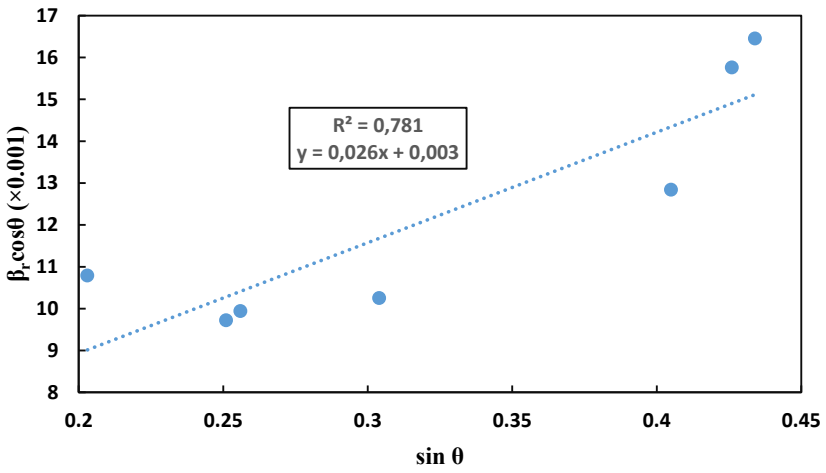

Fig. 2. Williamson-Hall plot of $CdWO_4$-RGO140 sample.

fitted line is attributed to lattice microstrains. The positive slope of the fitted line shows that a tensile microstrain is induced in the crystal lattice of the sample. Table 1 shows grain sizes and lattice microstrains for all samples. $CdWO_4$-RGO160 has the highest lattice tensile strain. The induced lattice strain is commonly originated from defects and lattice distortions in the crystals [35]. The small value for the pure $CdWO_4$ is due to absence of graphene.

The FT-IR spectra of $CdWO_4$ and $CdWO_4$- RGO samples were measured in the wavenumber region of 400-4000 cm^{-1} and are shown in Fig. 3. A symmetrical stretching vibrations of W-O-W bond in $[WO_4]^{2-}$ is represented by the band at 725 and 890 cm^{-1} [26]. The bending and stretching vibrations of Cd-O (580 cm^{-1}) and W-O (820 cm^{-1}) were also identified in the pure $CdWO_4$ and $CdWO_4$-RGO nanocomposites. The strong band centered at 1384 cm^{-1} is assigned to the symmetrical and asymmetrical vibrations of C-O bond. This peak is considerable in the nanocomposites that indicates presence of graphene oxide in the samples. By increasing the reaction temperature from 140 to 180°C, this peak is decreased which can be related to reduction of graphene oxides. The broad absorption band centered at 3430 cm^{-1} is attributed to the vibration of H-O bonds for surface hydration layers that is higher in the nanocomposite samples than the pure $CdWO_4$. The weak absorption located at 1635 cm^{-1} is associated with the deformation vibration of H-O-H bonds of water molecules, and centered peak at 2360 cm^{-1} related to C-H stretching vibration [36,37].

Table 1. Calculated average crystallite size and lattice microstrain for the samples.

Sample	*D* (nm)	*ε*
$CdWO_4$	64	$0.015\pm9\times10^{-7}$
$CdWO_4$-RGO140	38	$0.026\pm8\times10^{-5}$
$CdWO_4$-RGO160	20	$0.041\pm12\times10^{-5}$
$CdWO_4$-RGO180	55	$0.021\pm4\times10^{-5}$

Fig. 4 shows morphology of the different samples by SEM. It can be seen in the Fig. 4 (a) that the pure $CdWO_4$ sample has nanorods structures and these nanorods are distributed homogenously. From the images of nanocomposite samples in the Figs. 4(b)-(d), we can see $CdWO_4$ nanorods which have grown among RGO sheets. As shown in Fig. 4 (a), $CdWO_4$ nanorods in the pure sample have 50-100 nm diameter and ~1 µm length. By adding graphene to the nanocomposite samples, these dimensions are considerably decreased.

Fig. 5 shows TEM image of the pure $CdWO_4$ sample. The obtained $CdWO_4$ nanostructures appear to have uniform rod-like morphologies with 30–100 nm width. This result is corresponded with SEM image.

Raman spectroscopy is widely employed to study the ordered/disordered crystal structures of carbonaceous materials. According to the Fig. 6(a), Raman spectrum of the pure $CdWO_4$ has only one strong vibration at 896 cm^{-1} and several weak vibrations at 776, 705, 686 and 548 cm^{-1}. The vibration modes located at 896 cm^{-1} are correspond to the normal W–O vibrations of the

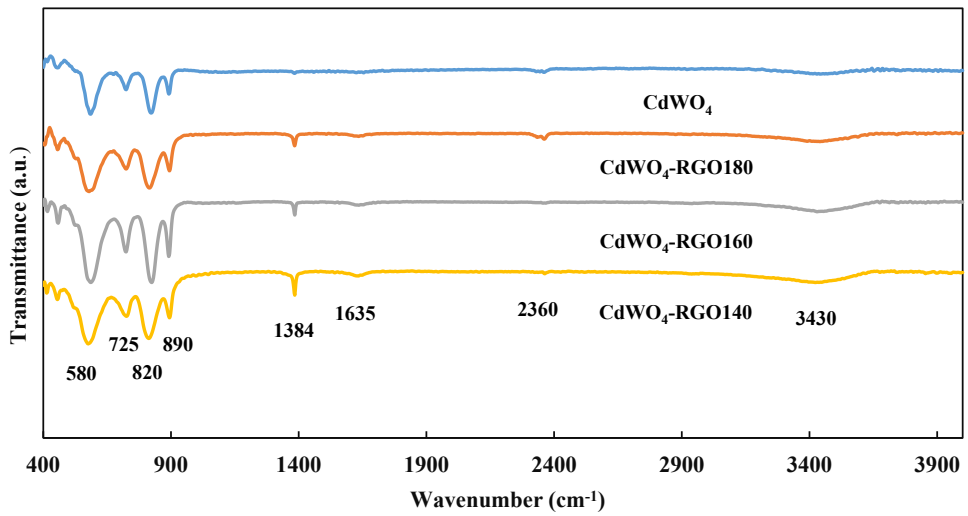

Fig. 3. FT-IR spectra of the pure $CdWO_4$ and $CdWO_4$-RGO140, 160 and 180 samples.

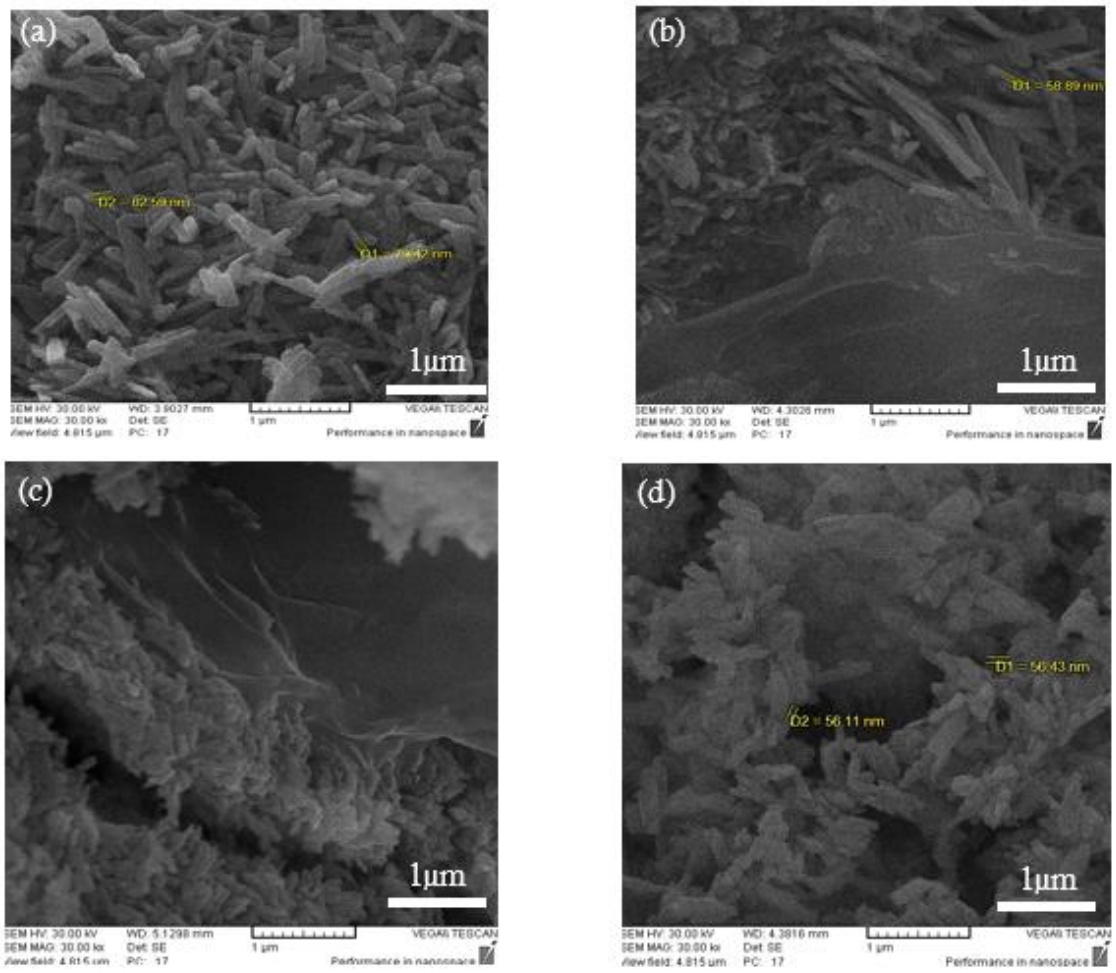

Fig. 4. SEM images of (a) the pure $CdWO_4$, (b) $CdWO_4$-RGO140, (c) $CdWO_4$-RGO160 and (d) $CdWO_4$-RGO180 samples.

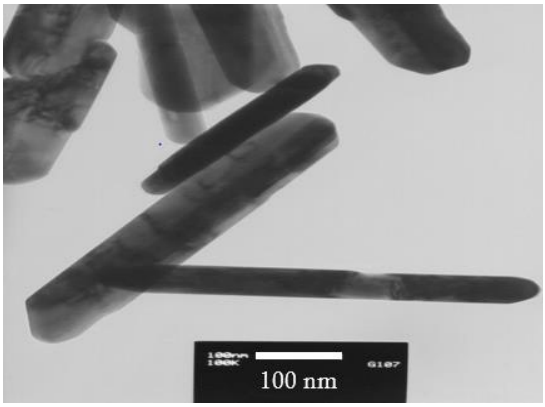

Fig. 5. TEM image of the pure $CdWO_4$ sample.

WO_6 octahedral, while the modes located at 776 and 686 cm^{-1} involve motions of WO_6 octahedral against the Cd^{2+} [38,39]. Bands in the range of 500–600 cm^{-1} are characteristic of symmetric W–O–W stretching modes [39]. Therefore, the Raman analysis confirmed that monoclinic $CdWO_4$ were successfully prepared. In Fig. 6(b), we can also see the Raman spectrum of $CdWO_4$-RGO160. The result is similar to the pure $CdWO_4$ but the intensity of peaks are declined. In addition, $CdWO_4$-RGO160 exhibited D line at 1318 cm^{-1} and G line at 1591 cm^{-1}. I_D/I_G (intensity ratio of D and G lines) is 1.46.

Fig. 7 shows the PL spectra of the pure $CdWO_4$ and $CdWO_4$-RGO nanocomposites. The obtained nanorods exhibit a very strong emission band in the range of 400–500 nm. The emission peak is at 450 nm for the pure $CdWO_4$. Moreover, it is at 451, 454 and 453 nm for $CdWO_4$-RGO140, $CdWO_4$-RGO160 and $CdWO_4$-RGO180, respectively. This PL emission is caused by the $^1A_1 \rightarrow {}^3T_1$ transitions

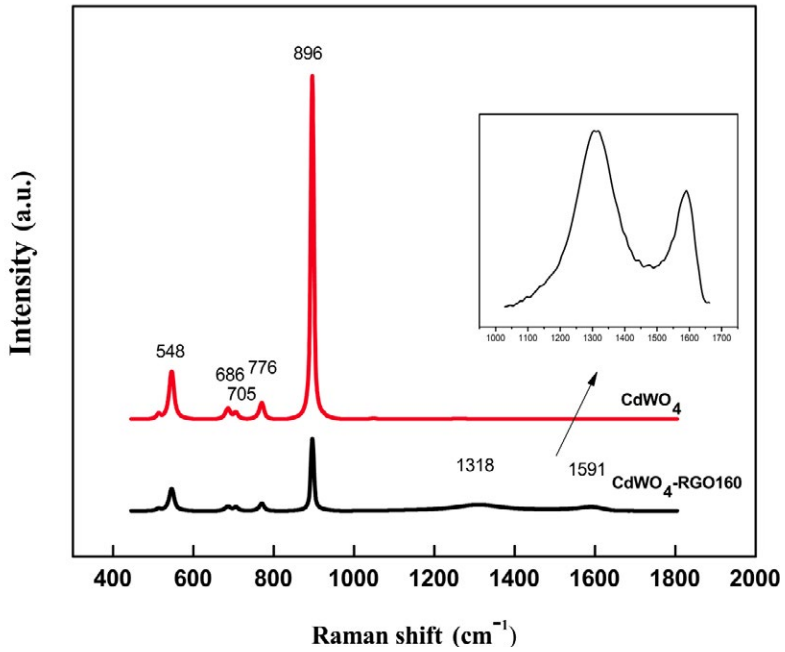

Fig. 6. Raman spectra of (a) the pure $CdWO_4$ and (b) $CdWO_4$-RGO160 samples.

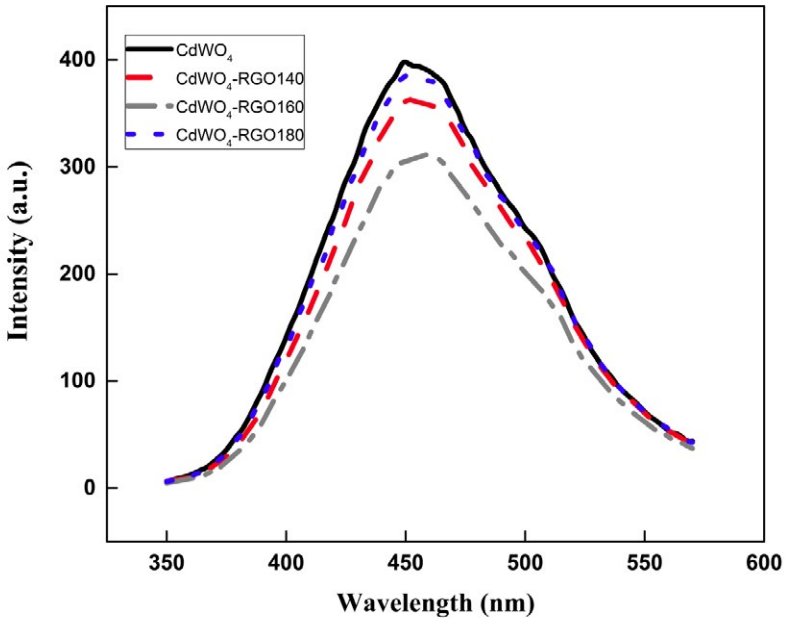

Fig. 7. Room-temperature PL spectra of the pure $CdWO_4$ and $CdWO_4$-RGO140, 160 and 180 nanocomposites.

within the WO_6^{6-} complex [40]. When RGO was added to $CdWO_4$, the photoemission intensity of the samples fell down due to quenching of photoemission. It can be seen from the figure that the highest intensity is related to the pure $CdWO_4$ and the lowest intensity is related to $CdWO_4$-RGO160. This indicates that photoelectron transfer from $CdWO_4$ to RGO in $CdWO_4$-RGO160 is more effective than others which impedes the recombination of photo induced electrons and holes.

As a main characterization of prepared samples, the photocatalytic properties of the pure $CdWO_4$ and $CdWO_4$-RGO nanocomposites have

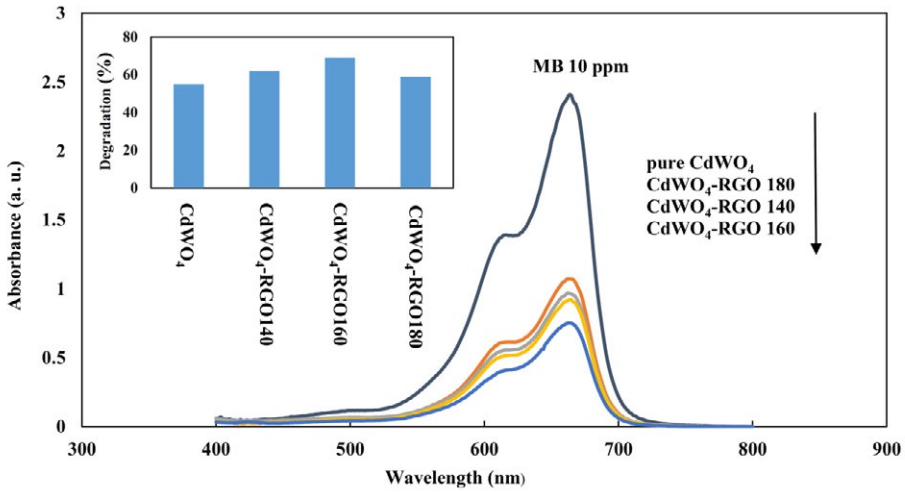

Fig. 8 The photocatalytic degradation of MB in the presence of the pure $CdWO_4$ and $CdWO_4$-RGO140, 160 and 180 samples after visible light irradiation for 180 min.

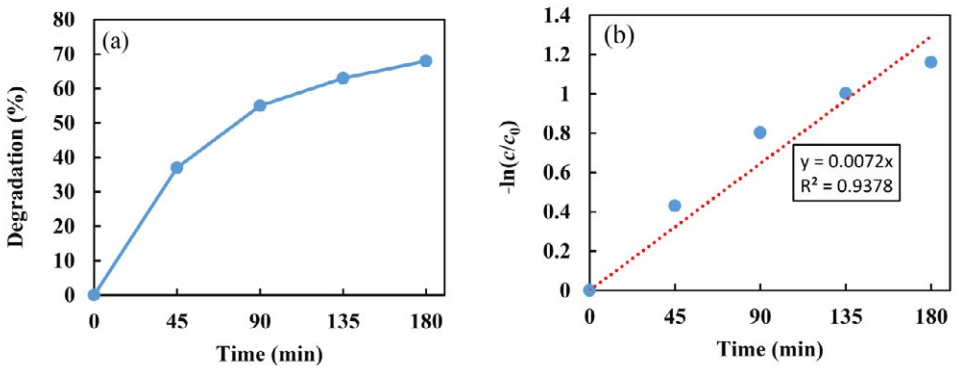

Fig. 9 (a) The photodegradation of MB vs. time and (b) the degradation rate constant with a first-order kinetic function for $CdWO_4$-RGO160 under visible light irradiation

been investigated and compared with each other. MB was considered as a model dye to evaluate the photocatalytic degradation performance of the samples. The photocatalytic activities of the as-prepared samples were investigated under visible light irradiation for 180 min to degradation of MB. The results are shown in the Fig. 8. Based on this figure, the activity of $CdWO_4$-RGO nanocomposites are better than the pure $CdWO_4$ and especially $CdWO_4$-RGO160 has the highest activity under the visible light irradiation. This activity can be related to the retardation of the recombination time in this sample which confirmed by PL results. By monitoring the MB absorption peak at 665 nm, the plots of the degradation percentage vs. reaction time were obtained for the pure $CdWO_4$ and $CdWO_4$-RGO nanocomposites under visible light irradiation. The MB degradation percentage was calculated by the following equation:

$$\text{Degradation (\%)} = \frac{c_0 - c}{c_0} \times 100 \qquad (2)$$

where c_0 and c are the initial and final concentrations of MB, respectively. This result is shown for $CdWO_4$-RGO160 in Fig. 9(a).

The kinetics of these degradation reactions were investigated, too. In order to calculate kinetics of degradation reactions, $-ln\frac{c}{c_0}=kT$ [42] relation was used, where c_0 is the initial concentration of a pollutant, c is MB concentration at time t, and k is the rate constant of the first-order reaction. The amount of k for $CdWO_4$-RGO160 can be obtained by determining the slope of ln c/c_0 vs. time (Fig. 9(b)). Table 2 shows the rate

Table 2. Rate constants of photodegradation for current work samples as compared to other works.

Sample	Pollutant	Light source	Rate constant (min^{-1})	Reference
$CdWO_4$	MB	Visible	0.0044	Current work
$CdWO_4$-RGO140	MB	Visible	0.0053	Current work
$CdWO_4$-RGO160	MB	Visible	0.0072	Current work
$CdWO_4$-RGO180	MB	Visible	0.0050	Current work
$CdWO_4$ nanorods	MB	UV	0.012	[31]
$CdWO_4$ nanorods	RhB	Visible	0.00991	[43]
$CdWO_4$ nanorods	RhB	Visible	0.00629	[44]
Bulk $CdWO_4$	MB	UV	0.0085	[45]

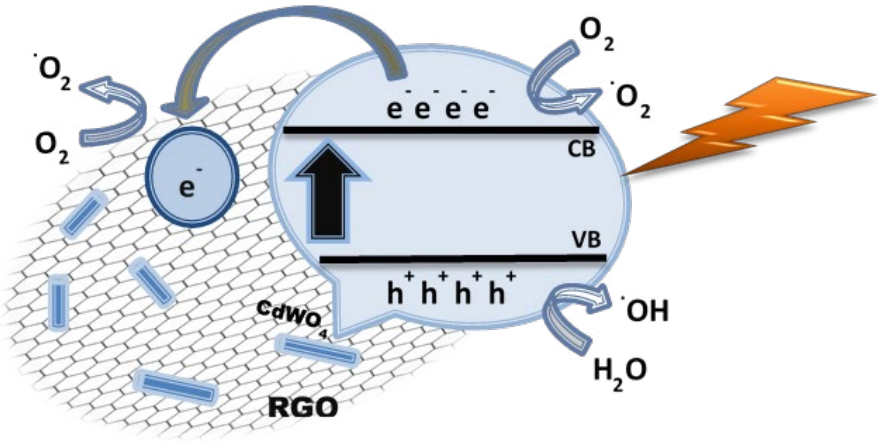

Fig. 10. Schematic presentation of the photocatalytic reactions on the nanocomposite samples.

constants of photodegradation for all samples of current work as compared to other works.

The charge separation and transfer in the reaction system of the nanocomposites are shown in Fig. 10. Under visible light irradiation, the excited electrons jump from the valence band (VB) of $CdWO_4$ nanorods to the conduction band (CB), and diffuse to the interface of $CdWO_4$ and RGO. With a good conductivity, RGO could be a good acceptor of photo-induced electrons. Hence, the recombination would be effectively suppressed and it has been confirmed by the PL results. As a result of this effect, much more holes (h^+) could diffuse to the surface of $CdWO_4$ and cause the formation of hydroxyl radicals ($^{\bullet}OH$), which subsequently degrade MB. Meanwhile, the transferred electrons might react with the dissolved oxygen to form the superoxide radicals ($^{\bullet}O_2$), which would also react with the dye molecules.

CONCLUSIONS

The hydrothermal method as an easy and feasible method was used for synthesizing the pure $CdWO_4$ and $CdWO_4$-RGO nanocomposites. Reaction hydrothermal temperature as 140, 160 and 180^{0}C have been investigated for $CdWO_4$-RGO nanocomposites. Synthesized samples contained $CdWO_4$ nanorods with lower than 100 nm diameter and 1 µm length. Raman spectra proved the presence of RGO in the nanocomposites. The photocatalysis experiment results showed that the $CdWO_4$-RGO nanocomposites have higher photocatalytic activity than the pure $CdWO_4$ sample for MB degradation. Among the nanocomposites, $CdWO_4$-RGO with reaction temperature of 160 ^{o}C had the best photocatalytic degradation effect and the lowest PL intensity due to the longest recombination time of photo-induced electrons and holes.

ACKNOWLEDGMENT

Authors would like to thank from Dr. S. Safa for his assistance and guidance in this research.

CONFLICT OF INTEREST

The authors declare that there are no conflicts of interest regarding the publication of this manuscript.

REFERENCES

1. Ansari F, Sobhani A, Salavati-Niasari M. PbTiO3/PbFe12O19 nanocomposites: Green synthesis through an eco-friendly approach. Composites Part B: Engineering. 2016;85:170-5.
2. Ansari F, Bazarganipour M, Salavati-Niasari M. NiTiO3/NiFe2O4 nanocomposites: Simple sol–gel auto-combustion synthesis and characterization by utilizing onion extract as a novel fuel and green capping agent. Materials Science in Semiconductor Processing. 2016;43:34-40.
3. Hoffmann MR, Martin ST, Choi W, Bahnemann DW. Environmental Applications of Semiconductor Photocatalysis. Chemical Reviews. 1995;95(1):69-96.
4. Linsebigler AL, Lu G, Yates JT. Photocatalysis on TiO2 Surfaces: Principles, Mechanisms, and Selected Results. Chemical Reviews. 1995;95(3):735-58.
5. Fujishima A, Rao TN, Tryk DA. Titanium dioxide photocatalysis. Journal of Photochemistry and Photobiology C: Photochemistry Reviews. 2000;1(1):1-21.
6. Zou Z, Ye J, Sayama K, Arakawa H. Direct splitting of water under visible light irradiation with an oxide semiconductor photocatalyst. Nature. 2001;414(6864):625-7.
7. Asahi R. Visible-Light Photocatalysis in Nitrogen-Doped Titanium Oxides. Science. 2001;293(5528):269-71.
8. Thompson TL, Yates JT. Surface Science Studies of the Photoactivation of TiO2New Photochemical Processes. Chemical Reviews. 2006;106(10):4428-53.
9. Wang X, Maeda K, Thomas A, Takanabe K, Xin G, Carlsson JM, et al. A metal-free polymeric photocatalyst for hydrogen production from water under visible light. Nature Materials. 2008;8(1):76-80.
10. Fujihira M, Satoh Y, Osa T. Heterogeneous photocatalytic oxidation of aromatic compounds on TiO2. Nature. 1981;293(5829):206-8.
11. Kudo A, Miseki Y. Heterogeneous photocatalyst materials for water splitting. Chem Soc Rev. 2009;38(1):253-78.
12. Kato H, Asakura K, Kudo A. Highly Efficient Water Splitting into H2and O2over Lanthanum-Doped NaTaO3Photocatalysts with High Crystallinity and Surface Nanostructure. Journal of the American Chemical Society. 2003;125(10):3082-9.
13. Markov S, Nagirnyi V, Vasil'ev A, Makhov V, Laasner R, Vielhauer S, et al. Modelling of decay kinetics of self-trapped exciton luminescence in CdWO4 under femtosecond laser excitation in absorption saturation conditions. Open Physics. 2012;10(4).
14. Yan J, Shen Y, Li F, Li T. Synthesis and Photocatalytic Properties of ZnWO4Nanocrystals via a Fast Microwave-Assisted Method. The Scientific World Journal. 2013;2013:1-8.
15. Dong T, Li Z, Ding Z, Wu L, Wang X, Fu X. Characterizations and properties of Eu3+-doped ZnWO4 prepared via a facile self-propagating combustion method. Materials Research Bulletin. 2008;43(7):1694-701.
16. Saito N, Sonoyama N, Sakata T. Analysis of the Excitation and Emission Spectra of Tungstates and Molybdate. Bulletin of the Chemical Society of Japan. 1996;69(8):2191-4.
17. Lotem H, Burshtein Z. Method for complete determination of a refractive-index tensor by bireflectance: application to CdWO_4. Optics Letters. 1987;12(8):561.
18. Pustovarov VA, Krymov AL, Shulgin BV, Zinin EI. Some peculiarities of the luminescence of inorganic scintillators under excitation by high intensity synchrotron radiation. Review of Scientific Instruments. 1992;63(6):3521-2.
19. Charpak G. Coupling of scintillators and gaseous detectors: a new approach to gamma-ray detectors. Gamma-Ray Detectors; 1992/12/22: SPIE; 1992.
20. Priya AM, Selvan RK, Senthilkumar B, Satheeshkumar MK, Sanjeeviraja C. Synthesis and characterization of CdWO4 nanocrystals. Ceramics International. 2011;37(7):2485-8.
21. Wang Y, Ma J, Tao J, Zhu X, Zhou J, Zhao Z, et al. Low-temperature synthesis of CdWO4 nanorods via a hydrothermal method. Ceramics International. 2007;33(6):1125-8.
22. Ye D, Li D, Chen W, Shao Y, Xiao G, Sun M, et al. Characterization and properties of Eu3+-doped CdWO4 prepared by a hydrothermal method. Research on Chemical Intermediates. 2009;35(6-7):675-83.
23. Ziluei H, Azimirad R, Mojtahedzadeh Larijani M, Ziaie F. Preparation and optimization of CdWO 4 -polymer nano-composite film as an alpha particle counter. Nuclear Instruments and Methods in Physics Research Section A: Accelerators, Spectrometers, Detectors and Associated Equipment. 2017;852:85-90.
24. Nadaraia L, Jalabadze N, Chedia R, Antadze M, Khundadze L. Preparation of Tungstate Nanopowders by Sol-Gel Method. IEEE Transactions on Nuclear Science. 2010;57(3):1370-6.
25. Jia R, Zhang G, Wu Q, Ding Y. Preparation, structures and photoluminescent enhancement of CdWO 4 – TiO 2 composite nanofilms. Applied Surface Science. 2006;253(4):2038-42.
26. Rondinone AJ, Pawel M, Travaglini D, Mahurin S, Dai S. Metastable tetragonal phase CdWO4 nanoparticles synthesized with a solvothermal method. Journal of Colloid and Interface Science. 2007;306(2):281-4.
27. Lim CS. Microwave-assisted synthesis of CdWO4 by solid-state metathetic reaction. Materials Chemistry and Physics. 2012;131(3):714-8.
28. Lou Z, Hao J, Cocivera M. Luminescence of ZnWO4 and CdWO4 thin films prepared by spray pyrolysis. Journal of Luminescence. 2002;99(4):349-54.
29. Wang Y, Ma J, Tao J, Zhu X, Zhou J, Zhao Z, et al. Morphology-controlled synthesis of CdWO4 nanorods and nanoparticles via a molten salt method. Materials Science and Engineering: B. 2006;130(1-3):277-81.
30. Liao H-W, Wang Y-F, Liu X-M, Li Y-D, Qian Y-T. Hydrothermal Preparation and Characterization of Luminescent CdWO4Nanorods. Chemistry of Materials. 2000;12(10):2819-21.
31. Xu J, Chen M, Wang Z. Preparation of CdWO4-deposited reduced graphene oxide and its enhanced photocatalytic properties. Dalton Transactions. 2014;43(9):3537.
32. Safa S, Sarraf-Mamoory R, Azimirad R. Investigation of reduced graphene oxide effects on ultra-violet detection of ZnO thin film. Physica E: Low-dimensional Systems and Nanostructures. 2014;57:155-60.
33. Ye D, Li D, Zhang W, Sun M, Hu Y, Zhang Y, et al. A New Photocatalyst CdWO4 Prepared with a Hydrothermal Method. The Journal of Physical Chemistry C. 2008;112(44):17351-6.
34. Vaseem M, Umar A, Hahn YB, Kim DH, Lee KS, Jang JS, et al. Flower-shaped CuO nanostructures: Structural, photocatalytic and XANES studies. Catalysis Communications. 2008;10(1):11-6.
35. Vimalkumar TV, Poornima N, Kartha CS, Vijayakumar KP. Effect of precursor medium on structural, electrical and optical properties of sprayed polycrystalline ZnO thin films. Materials Science and Engineering: B. 2010;175(1):29-35.
36. Li G, Li L, Boerio-Goates J, Woodfield BF. High Purity

Anatase TiO2Nanocrystals: Near Room-Temperature Synthesis, Grain Growth Kinetics, and Surface Hydration Chemistry. Journal of the American Chemical Society. 2005;127(24):8659-66.
37. Huang G, Zhu Y. Synthesis and photocatalytic performance of ZnWO4 catalyst. Materials Science and Engineering: B. 2007;139(2-3):201-8.
38. Lacomba-Perales R, Errandonea D, Martinez-Garcia D, Rodríguez-Hernández P, Radescu S, Mujica A, et al. Phase transitions in wolframite-typeCdWO4at high pressure studied by Raman spectroscopy and density-functional theory. Physical Review B. 2009;79(9).
39. Daturi M, Busca G, Borel MM, Leclaire A, Piaggio P. Vibrational and XRD Study of the System CdWO4−CdMoO4. The Journal of Physical Chemistry B. 1997;101(22):4358-69.
40. Polak K, Nikl M, Nitsch K, Kobayashi M, Ishii M, Usuki Y, et al. The blue luminescence of PbWO4 single crystals. Journal of Luminescence. 1997;72-74:781-3.
41. Safa S, Azimirad R, Safalou Moghaddam S, Rabbani M. Investigating on photocatalytic performance of CuO micro and nanostructures prepared by different precursors. Desalination and Water Treatment. 2015;57(15):6723-31.
42. Cao QW, Cui X, Zheng YF, Song XC. A novel CdWO4/BiOBr p–n heterojunction as visible light photocatalyst. Journal of Alloys and Compounds. 2016;670:12-7.
43. Wen X-J, Niu C-G, Zhang L, Huang D-W, Zeng G-M. In-situ synthesis of visible-light-driven plasmonic Ag/AgCl-CdWO4 photocatalyst. Ceramics International. 2017;43(2):1922-9.
44. Li D, Bai X, Xu J, Ma X, Zhu Y. Synthesis of CdWO4nanorods and investigation of the photocatalytic activity. Phys Chem Chem Phys. 2014;16(1):212-8.